Sorption mechanisms of lead on soil-derived black carbon formed under varying cultivation systems

Qingjie Zhao [a,1], Jianhong Li [a,b,1], Binoy Sarkar [c], Weidong Wu [a], Boling Li [a], Ruichun Liu [d], Mohsin Nawaz [e], Muhammad Zia-ur-Rehman [f], Hailong Wang [b,g,], Zhipeng Wu [a,*]**

[a] College of Tropical Crops, Hainan University, Haikou 570228, China

[b] Biochar Engineering Technology Research Center of Guangdong Province, School of Environmental and Chemical Engineering, Foshan University, Foshan 528000, China

[c] Lancaster Environment Centre, Lancaster University, Lancaster, LA1 4YQ, United Kingdom

[d] Flood Control and Drought Relief Office of Hangjin County, Ordos 017400, China

[e] Key Laboratory of Genetics and Germplasm Innovation of Tropical Special Forest Trees and Ornamental Plants, Ministry of Education, College of Forestry, Hainan University, Haikou 570228, China

[f] Institute of Soil and Environmental Sciences, University of Agriculture, Faisalabad, 38040, Pakistan

[g] Key Laboratory of Soil Contamination Bioremediation of Zhejiang Province, Zhejiang A&F University, Hangzhou 311300, China

[*] Corresponding author.

[**] Correspondence to: H. Wang, School of Environmental and Chemical Engineering, Foshan University, Foshan 528000, China

E-mail addresses: hailong.wang@fosu.edu.cn (H. Wang), peter@hainanu.edu.cn (Z. Wu).

[1] Qingjie Zhao and Jianhong Li contributed to the work equally and should be considered co-first authors.

Highlights

- Cultivation intensities of soils significantly affect black carbon characteristics.
- High cultivation intensity increased Pb in ion exchange fraction on black carbon.
- Ion exchange and hydrogen bonded Pb fractions accounted for about 80% of total Pb.
- Black carbon had high potential to retain Pb in stable form (by 18.7 - 21.1 mg kg^{-1}).
- Pb amount in ion exchange fraction was highly correlated with CEC of black carbon.

Graphical abstract

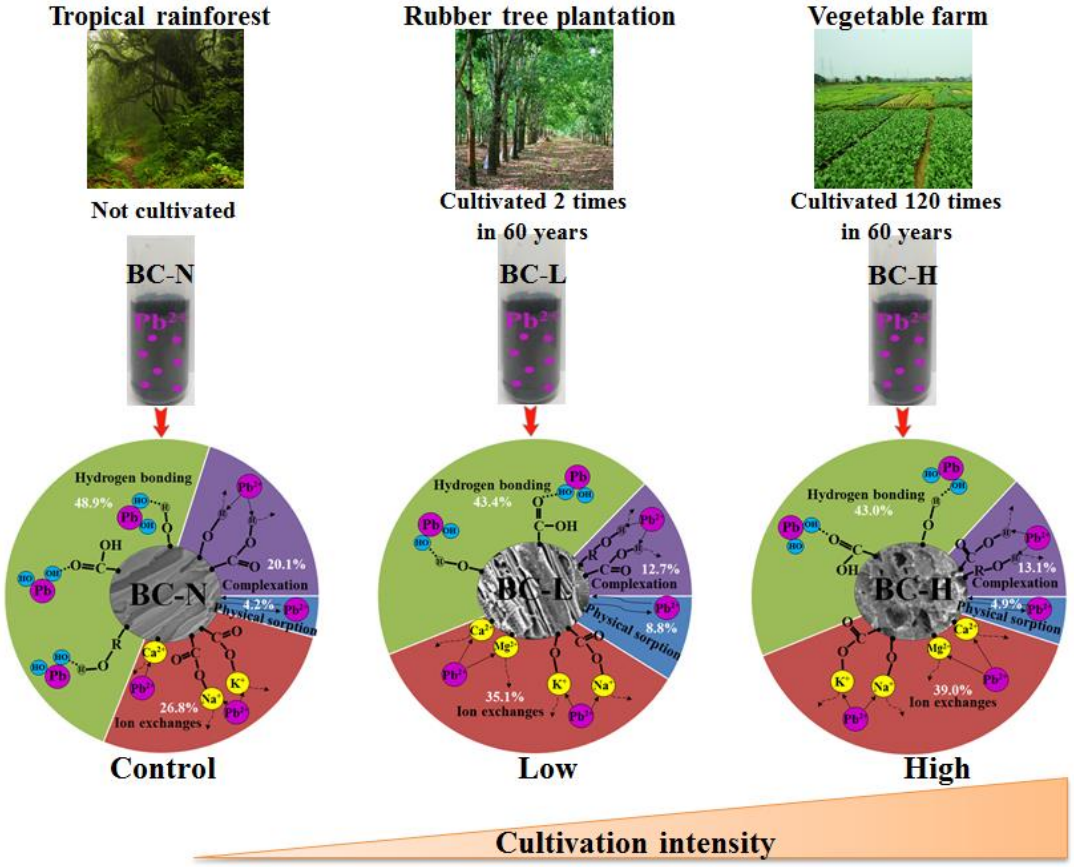

Abstract

The knowledge about lead (Pb) sorption on soil-derived black carbons (SBCs) under different cultivation intensities of soils is limited. In this study, chemical and spectroscopic methods were applied to investigate the Pb sorption mechanisms on SBCs in soils from a forest land, a rubber plantation area, and a vegetable farm with none, less and highly intensive cultivation, respectively, that are located in the Hainan Island of China. Results showed that the specific surface area and cation exchange capacity of the SBCs from the less and highly intensive cultivation soils were 4.5- and 2.7-fold, and 1.3- and 1.8-fold higher compared to that of SBC from the no-cultivation soil, which subsequently enhanced the Pb sorption capacities of SBCs in iron exchange fraction. Ion exchange and hydrogen bonded Pb fractions together accounted for about 80% of total Pb sorbed on all SBCs at an externally added 1,000 mg L^{-1} Pb solution concentration. The O=C−O groups also played key roles in Pb sorption by forming complexes of O=C−O−Pb−O and/or O=C−O−Pb. Overall, SBCs in soils under all studied cultivation intensities showed high potential to sorb Pb (with the maximum absorbed Pb amount of 46.0 to 91.3 mg g^{-1}), and increased Pb sorption capacities of the studied soils by 18.7 - 21.1 mg kg^{-1} in the stable fraction (complexation). Therefore, SBC might be a potential environment-friendly material to enhance the Pb immobilization capacity of soil.

Keywords: Aging of organic carbon; biochar; sequential desorption; TG/DTG; XPS.

Abbreviations: SBC: soil-derived black carbon; BC: black carbon; SOC: soil organic carbon; SSA: specific surface area; CEC: cation exchange capacity; ICP-MS: inductively coupled plasma mass spectrometer; PTEs: potentially toxic elements; TG/DTG: thermogravimetric and differential thermogravimetric; XPS: X-ray photoelectron spectroscopy.

1. Introduction

Sorption of potentially toxic elements (PTEs) on solid matrices such as soils and sediments is one of the key components which determine the fate and behavior of PTEs in the environment (Chiou, 2002; Shaheen et al., 2013). It has been recognized that various forms of soil organic matter (SOM) could serve as dominant environmental "compartments" for the sorption and accumulation of PTEs (Zhou et al., 2018). Black carbon (BC) serves as a chemically and biologically stable form of SOM which exists in the soil over a long period (Liang et al., 2008; Qi et al., 2017). As one form of BCs, biochar has been found to be an excellent material for adsorption of organic pollutants (Qin et al., 2018; Zhang et al., 2019; Chen et al., 2020a) and PTEs (Ali et al., 2020; Imran et al., 2020; Yin et al., 2020). The BC may significantly affect the sorption and immobilization of PTEs in soils in a wide range of biogeochemical processes (Liang et al., 2006; Qi et al., 2017), and could be regarded as an eco-friendly and potential material to immobilize PTEs in soil (Nie et al., 2018; Bandara et al., 2020; Wei et al., 2020). Therefore, the sorption capacity and the specific mechanisms of BC for metal ion retention are of great importance in remediation of contaminated soils.

Biomass-derived BC exists ubiquitously in soils to varying extents as a result of deliberate vegetation burning, wildfires or emissions from energy production units (Schmidt and Noack, 2000). For example, the 2019-20 fire season in eastern Australia is attracting considerable international attention where millions of ha of temperate forest areas have been burnt during the fire (Nolan et al., 2020). It has caused serious ecological damage, along with that a large amount of charcoal, the product of the incomplete combustion of vegetation (Pereira et al., 2014), was produced. Aging of charcoals (a fraction of BCs) in the soil results in the formation of persistent soil organic carbon (SOC) (Bennett et al., 2020), including soil-derived black carbon (SBC). The SBCs from natural formation or artificial amendments, however, have high specific surface area (SSA), high cation exchange capacity (CEC), and various organic functional groups. These characteristics might increase the

sorption capacity of PTEs on SBC during the PTE remediation processes (Qi et al., 2017). In recent years, artificial BC such as biochar has been successfully applied as a highly efficient soil amendment to immobilize PTEs (Liu et al., 2018; Li et al., 2019a; Li et al., 2020).

Exploration of the sorption and immobilization potential of PTEs by natural BC in soils is also immensely important since the global BC stock in waters, sediments, and soils combined is 300 to 500 giga–metric tons of carbon (Jaffé et al., 2013). Previous studies reported that aging of biochar following soil application changes its physiochemical properties while forming a range of biochar-derived organic materials (Mia et al., 2017). Moreover, crop cultivation practices can increase the association of charcoal with soil minerals, e.g., silicates, phosphates, aluminum oxides, and iron oxides in soils, thereby changing the elemental characteristics of charcoal (Hardy et al., 2017). The above changes in elemental compositions cause a modification of the physiochemical properties of charcoals and BC affecting their capacity to immobilize PTEs (Bandara et al., 2020). Few studies also claim that intensive cultivation of soils can change the PTE retention efficiency of SBC (Zahedifar, 2017).

It is difficult for agricultural and forestry soils to avoid PTE pollution in the process of land development and utilization due to a rapid development of social economy, industry and urbanization. Unraveling the sorption characteristics and mechanisms of PTEs on SBC from agricultural and forestry soils can help exploring the potential of BC or biochar in influencing the immobilization of PTEs in agricultural and forestry lands. The natural tropical rainforest in the Bawangling Forest Region (108.88°-109.33°E, 18.86°-19.20°N) of Hainan island in China (Lu et al., 2018) was rarely disturbed for replacing its plantations, and has therefore existed for several thousand years without any cultivation (Zhang et al., 2010; Wang et al., 2017a), except a serious damage caused by people for creating more farmland or for obtaining more forest resources about 600 years ago in the Ming Dynasty (Dodson et al., 2019). The lands nearby the Bawangling Forest Region have been cultivated for

about 60 years (Lu et al., 2018). Rubber trees near the Bawangling Forest Region was adopted as the secondary plantation under less intensive cultivation (cultivated about 20 years ago) system, while vegetables were grown twice a year in some lands under highly intensive cultivation system. It could be hypothesized that the physicochemical properties (e.g., CEC, elemental composition and organic functional groups) of SBCs under the less intensive cultivation system would be significantly different from those of the highly intensive cultivation system and no cultivation system, which would further affect the sorption capacities and mechanisms of Pb (a representative PTE) by SBCs from these systems.

The sorption mechanisms of PTEs on artificial BC (e.g., biochar) in aqueous solutions have been reported extensively (Li et al., 2019b; Yang et al., 2019; Fang et al., 2020). The major mechanisms involved in the removal of PTEs from aqueous solutions using biochars were ion-exchange, electrostatic attraction, outer-sphere and/or inner-sphere complexation, surface precipitation and/or co-precipitation (Wang et al., 2019). Several methods including potentiometric titration, sequential extraction, thermal analysis techniques such as thermogravimetric (TG) and differential thermogravimetric (DTG) analyses, and X-ray photoelectron spectroscopy (XPS) have been proven as useful methods to study the characteristics of organic functional groups and thermal stability of organic components on BCs, and analyze the interactions between carbon-based adsorbents and PTE adsorbates (Plante et al., 2009; Li et al., 2019b; Xia et al., 2019). These methods were used to investigate Pb sorption characteristics and mechanisms of SBCs from different soils in the current study.

In this study, we separated three SBCs from the soils under different cultivation systems (i.e., no-cultivation, less intensive cultivation, and highly intensive cultivation) in the Hainan island of China to conduct Pb sorption and desorption experiments on SBCs. The specific objectives of this work are to: (1) characterize the elemental composition and physicochemical properties of the SBCs; (2) explore sorption and desorption characteristics of SBCs for Pb; and (3) investigate the sorption mechanisms of Pb onto SBCs.

2. Materials and methods

2.1. Soil collection and separation of black carbon

Three surface soils (0–20 cm depth) were collected in triplicate from the three sampling sites (without any artificial black carbon added), including a natural tropical rainforest (109.09°E, 19.13°N) in the Bawangling Forest Region (Hainan Province of China), a rubber tree plantation area (109.50°E, 19.53°N), and a vegetable farm (109.57°E, 19.48°N) near the Bawangling Forest Region. The three collected soil samples represented no-cultivation, less intensive cultivation and highly intensive cultivation systems, respectively, and referred to as Soil 1, Soil 2 and Soil 3. Following sample collection, soil pH was determined in a soil suspension (soil:water = 1:2.5(w/v)) according to Li et al. (2020), while soil organic carbon was determined using the $K_2Cr_2O_7$ method (Bao, 2000). The pH value of Soil 1, Soil 2 and Soil 3 was 4.53, 4.98 and 4.64, while the soil organic carbon content was 31.01, 12.15 and 9.10 g kg^{-1}, respectively. The clay, silt, and sand particles were 13, 24 and 63%, and 18, 37 and 45% in Soil 1 and Soil 2, respectively. The soil particle fractions with particle size less than 10 μm, between 10 and 50 μm, and greater than 250 μm were 33.0, 23.2 and 43.8%, 40.8, 29.4 and 29.8%, and 13.7, 56.8 and 29.5% in Soil 1, Soil 2 and Soil 3, respectively.

The SBC particles (with diameter > 0.5 mm) were selected and picked from Soil 1 (no-cultivation), Soil 2 (less intensive cultivation) and Soil 3 (highly intensive cultivation) using superfine stainless forceps according to Dong et al. (2017), and referred to as BC-N, BC-L and BC-H, respectively. The SBC particles were suspended into deionized water at a ratio of 1:10 (w/v) and shaken slightly to remove soil particles adhered to the SBC particles. The SBC particles were then washed three times with deionized water, and put in a 60 °C drying oven until the weight of the particles reached a constant value (Koide et al., 2011). All SBC particles were ground and passed through a 0.15 mm sieve, and stored for further use.

146

147 **2.2. Preparation of Pb-loaded black carbon**

148 Lead-loaded SBCs were prepared by adding 1.0 g of SBC into 500 mL of 10, 20, 40, 80, 150, 300, 600 and
149 1000 mg L^{-1} of Pb aqueous solutions (by dissolving analytical grade $Pb(NO_3)_2$) at pH 5.0 in Erlenmeyer flasks.
150 Ucun et al. (2003) reported Pb precipitation ($Pb(OH)_2$) at pH 5.5. In this study, the pH value of solutions was
151 selected at 5.0 since the pH of the studied soils ranged from 4.5 to 5.0. The flasks were capped with rubber plugs,
152 agitated on a thermostatic reciprocating shaker at 220 rpm (25 °C) for 24 h. Then, the aqueous solutions were
153 filtered through a 0.45 μm cellulose-acetate membrane filter paper, and the residual Pb-loaded SBCs was
154 washed with deionized water, and air-dried at room temperature prior to further analysis.

155

156 **2.3. Characterization of black carbon**

157 Total hydrogen (H), carbon (C), and nitrogen (N) contents of SBCs were measured using an elemental
158 analyzer (Vario ELIII - Elementary Company, Germany). The oxygen (O) content was calculated by the
159 difference assuming that the SBC was composed only of H, C, N, and O (Wu et al. 2012). Ash content of the
160 SBCs was determined by placing crucibles containing the samples in a muffle furnace at 750°C for 6 h
161 (D1762-84, 2007). The crucibles were kept with lids in a desiccator for 1 h for cooling, and then weighed. Pore
162 volume and SSA of SBCs were measured by N_2 adsorption isotherms (ASAP2460, Micromeritics, USA)
163 applying the Brunauer-Emmett-Teller (BET) equation (Brunauer et al., 1938). The contents of acidic functional
164 groups of SBCs were determined by the Boehm titration method (Boehm, 1994). The CEC of SBCs was
165 determined following 1 M ammonium acetate (pH 7) extraction method (Wu et al., 2017). In order to measure
166 total carbon content of SBCs in soils, soil samples were digested using peroxide to remove non-BC. Twenty
167 grams of air-dried soil was treated with 30% (w/w) peroxide (initially 10 mL, with daily additions up to a total

of 30–50 mL until no further bubbles appeared), and heated on a hot plate at 90 °C to ensure maximum non-BC removal (Liang et al., 2006). Total carbon content of SBCs in soils was then measured using the $K_2Cr_2O_7$-heating method (Bao, 2000). The total carbon content of BC-N, BC-L and BC-H in Soil 1, Soil 2 and Soil 3 was 0.81, 1.58 and 1.08 g kg^{-1}, therefore, the weight content of BC-N, BC-L and BC-H in the soils was 1.65, 3.30 and 2.36 g kg^{-1}, respectively ($W_{BC} = T_{BC} \times E_{C\%}$, while W_{BC}, T_{BC} and $E_{C\%}$ refer to weight content of SBCs in soils, total carbon content of SBCs in soils, and carbon percentage of SBCs, respectively).

Thermogravimetric (TG) and differential thermogravimetric (DTG) analyses curves were obtained using a thermogravimetric analyzer (SDT Q600, TA Instruments, USA) at a heating rate of 10 °C min^{-1} from 30 °C to 1000 °C under a controlled atmosphere of N_2 (50 mL min^{-1}) with an initial material mass of 30 mg. Fourier transform infrared (FTIR) analysis of SBCs before Pb sorption was conducted according to Wu et al. (2016). Spectra were collected using a TENSOR 27 FTIR spectrophotometer (Bruker Company, Germany) scanning from 4000 to 400 cm^{-1} (wavenumber) at a resolution of 2 cm^{-1}. The X-ray photoelectron spectroscopy (XPS, AXIS SUPRA, Japan) was used to measure the bonding energies of C, O, and Pb on the SBCs and Pb-loaded SBCs prepared at 1000 mg L^{-1} Pb aqueous solution (scans for C 1s, O 1s and Pb 4f). Samples were freeze-dried, ground to powder in the anaerobic chamber, and pressed into pellets. The energy range was 0−1000 eV for wide-scan spectra (Li et al., 2020).

2.4. Sorption experiments

A stock solution of 1000 mg L^{-1} Pb was prepared by dissolving $Pb(NO_3)_2$ in 0.01 M $NaNO_3$ solution. Sorption kinetics was determined by determining sorption amounts at various time intervals (5, 10, 15, 20, 30, 40, 60, 120, 240, 480, 960 and 1440 min) at pH 5.0. The pH value of suspension was adjusted with 0.1 M NaOH or 0.1 M HNO_3 solution to simulate a typical soil water situation (Li et al., 2019b). Sorption isotherm

190 experiments were carried out with different initial Pb concentrations (10, 20, 40, 80, 150, 300, 600 and 1000 mg
191 L^{-1}) at pH 5.0. Both sorption kinetics and isotherm experiments involved an adsorbent suspension with a
192 SBC:solution ratio of 1:25 (w/v) in 50 mL tubes (Wu et al., 2017). These tubes were agitated on a rotating
193 shaker at 220 rpm and 25 °C for 24 h. The solutions were filtered (< 0.45 μm filter) and preserved in test tubes
194 (Li et al., 2019b). Concentrations of Pb in the filtrates were measured using an inductively coupled plasma mass
195 spectrometer (ICP-MS, Thermo Fisher-X series, USA). The released alkali or alkaline earth metals (such as Na^+,
196 K^+, Mg^{2+} and Ca^{2+}) from the original SBCs in the supernatant (under Pb concentration of 1000 mg L^{-1}) were
197 also analyzed by ICP-MS. The corresponding release of Na^+, K^+, Mg^{2+} and Ca^{2+} from the SBCs with deionized
198 water (at the same pH) served as the control. All treatments in the sorption experiments were conducted in
199 triplicate.
200
201 **2.5. Desorption experiments**
202 Lead fractionation in Pb-loaded SBCs (prepared in section 2.2 of this study) during desorption experiments
203 was conducted using the method modified from Andreas and Zhang (2014). The sorbed Pb was fractionated into
204 (i) physical sorption, (ii) ion exchange, (iii) hydrogen bonding, and (iv) complexation fractions. The physical
205 sorption fraction is affected by van der Waals force between Pb and SBC surface, ion exchange fraction is
206 attributed to the cation exchange between Pb and other cations on SBC surface, hydrogen bonding fraction is
207 formed by hydrogen bonds between Pb forming hydrates [$Pb(H_2O)_6^{2+}$] and oxygen-containing functional groups
208 on SBC surface, and complexation fraction is influenced by coordination reaction of Pb on SBCs surface
209 (Andreas and Zhang, 2014). Accordingly, 0.05 g of Pb-loaded SBC was added into a 50 mL plastic tube. All
210 tubes with samples were placed on a reciprocating shaker at 25 °C and rotated at 220 rpm, and then sequentially
211 extracted with (i) 25 mL ultrapure water shaking for 2 h, (ii) 8 mL CH_3COONH_4 (1 M, pH=7) shaking for 6 h,

(iii) 10 mL CH_3COOH (4.37 M) + $NH_2OH{\cdot}HCl$ (0.04 M) shaking for 5 h, and (iv) 10 mL sodium pyrophosphate (0.1 M) shaking for 5 h, respectively, to determine the above four Pb fractions. The suspensions were centrifuged at 5000 rpm for 20 min (at 25 °C) using a centrifuge machine (H2050R, Cence, China), and filtered using 0.45 μm cellulose-acetate membrane filters. Lead concentrations in the filtrates were measured using ICP-MS.

The sorption kinetics of Pb onto SBC was analyzed by the pseudo-first-order and pseudo-second-order models, the sorption isotherms of Pb onto SBCs were analyzed by the Langmuir and Freundlich models (Text S1 of the Supporting Information).

The Pb sorption capacity of the SBCs in physical sorption fraction (Q_{phy}), ion exchange fraction (Q_{exc}), hydrogen bonding fraction (bond with oxygen-containing function groups, Q_{hyd}), complexation fraction (Q_{com}) and total sorption fraction (Q_{tot}) were calculated by the Langmuir model fitting.

2.6. Statistical analysis

Results were expressed on a dry mass basis, and shown as mean ± standard deviation (SD) of three replicates per treatment. The standard deviation bars of results were added in specific figures. The fitting of the Langmuir and Freundlich models, pseudo-first-order and pseudo-second-order models, and the graphing of XPS spectra were done using the software Origin 9.0 (Origin Lab, USA).

3. Results and discussion

3.1. Properties of soil-derived black carbons

Elemental properties of the SBCs are shown in Table 1. The N content of SBCs increased 1.25- and 2.23-fold in Soil 2 (BC-L) and Soil 3 (BC-H) under the low and high cultivation intensity compared to that in

Soil 1 (BC-N) under no cultivation (the control). Values were presented by 1.64 and 2.36% N contents of BC-L and BC-H, respectively, while 0.73% for BC-N (the control). The H and O contents of SBCs were slightly increased with the increasing cultivation intensity from the control (3.61 and 46.5%) to low (3.87 and 46.6%) and high (3.90 and 47.8%) (Table 1). However, the C content slightly decreased (49.1, 47.9 and 45.9% C contents of BC-N, BC-L and BC-H, respectively) under the elevated cultivation intensity (Table 1). This might be attributed to the enhanced disturbances of soils and weathering of SBCs by various cultivation practices, e.g., ploughing, wetting and drying, and water and fertilizer management (Hardy et al., 2017). During farming of the land, the above practices inputted more N into the soil than the no-cultivation system, and accelerated the decomposition of BCs in the soil by bringing down the C:N ratio (Hardy et al., 2017). As a result, labile C-containing groups such as aromatic and aliphatic groups of SBCs were decomposed by microorganisms (Kuzyakov et al., 2009). Meanwhile, an increasing proportion of H and O-rich functional groups such as carboxyl, carbonyl and O-alkyl were formed on SBCs during the BC mineralization (Kuzyakov et al., 2009; Mia et al., 2017). Additionally, a high proportion of N-containing groups could increase the reaction ratio of positively charged N-containing functional groups in soil to negatively charged C-containing functional groups on SBCs under a high cultivation intensity (Hardy et al., 2017; Mia et al., 2017; Wang et al., 2018). This might contribute to the increase in N content of SBCs with increasing soil cultivation intensity. Similarly, Hardy et al. (2017) reported that charcoal in cropland over long cultivation time had higher O and H contents and N-alkyl groups than short cultivation duration due to enhanced weathering of various C substrates.

The higher the ratio of H/C and O/C in SBC, the lower is the aromaticity of SBC, and the more abundant is the organic functional groups such as hydroxyl and carboxyl groups (Wu et al., 2012; Wu et al., 2016). The order of H/C and O/C ratios of SBCs was: BC-H > BC-L > BC-N (Table 1). Thus, the H/C and O/C ratios increased under elevated weathering and cultivation disturbances of SBCs. These might be attributed to the

256 increased phenol, carbonyl and carboxyl functional groups which were created by the oxidation of SBC surfaces
257 during the aging of BCs under high cultivation intensity (Cao et al., 2019). The total content of acidic functional
258 groups (the sum of carboxylic acid (RCOOH), weak acid ester (RCOR'), and phenolic hydroxyl groups (AOH))
259 in BC-H (1.70 mmol g^{-1}) and BC-L (1.71 mmol g^{-1}) was higher than that of BC-N (1.57 mmol g^{-1}; Table 1),
260 which also indicated that hydroxylation and carboxylation of SBCs could be enhanced by increased cultivation
261 intensity and aging. As reported by Mukherjee et al. (2014), the advanced oxidation of SBCs most likely created
262 phenol, carboxyl and carbonyl functional groups at the edge of aromatic rings on the surfaces. Mia et al. (2017)
263 found that progressive aging of biochar (artificial BC) also led to a gradual formation of surface functional
264 groups such as phenolic, carboxyl, and carbonyl groups. The results of this study are consistent with those of
265 previous studies, showing that aging of charcoals in soil resulted in the oxidation of their surfaces (Lehmann et
266 al., 2005; Hardy et al., 2017). Accordingly, both H/C and O/C ratios of charcoal could be increased through
267 elevated aging intensities (Cheng et al., 2008; Pereira et al., 2014).

268 The CEC of three SBCs ranged from 128–227 cmol kg^{-1} (Table 1) with the order of BC-H (227.3 cmol
269 kg^{-1}) > BC-L (166.4 cmol kg^{-1}) > BC-N (128 cmol kg^{-1}). Under the low and high cultivation intensity of the
270 soils, a gradual aging resulted in the value of SSA of BC-L and BC-H to be 4.5- and 2.7-fold higher than that of
271 BC-N (Table 1). Thus, more sorption sites might be presented on the surface of BC-L and BC-H than BC-N,
272 which could increase CEC of SBCs. The higher total content of acidic functional groups of BC-L and BC-H
273 might also be responsible for the increase in CEC compared to that of BC-N in this study. Similarly, previous
274 studies reported that CEC of charcoal increased over increasing aging intensity (Cheng et al., 2008). The CEC,
275 variety of active functional groups and SSA were reported to affect the sorption capacities of biochar toward
276 PTEs, including Pb sorption and immobilization (Lu et al., 2017; Wu et al., 2017; Li et al., 2019b).

277 The peak intensity of functional groups on SBCs including the aromatic ring C=O stretching of β-diketone

ligands (1620–1580 cm^{-1}) (Li et al., 2019b), and cyclic anhydride C−O−C stretching (1300–1199 cm^{-1}) (Li et al., 2019b; Mumtaz et al., 2019) vibrations decreased with increasing cultivation intensity (Fig. 1), while the intensity of aliphatic C–H asymmetric stretching (2920 cm^{-1}), R–CH_3 symmetric stretching (2850 cm^{-1}) (Chen et al., 2020b), and non-cyclic anhydride C−O−C stretching (1150–1060 cm^{-1}) vibrations increased (Fig. 1). These changes were contributed likely by the hydrolyzation or decomposition of cyclic anhydride of carboxylic acid, and formation of C–H and R–CH_3 contained functional groups on SBCs during the increased cultivation intensity of the soils.

3.2. Sorption and desorption of Pb from Pb-loaded SBCs

The kinetics of Pb sorption on the three SBCs at pH of 5.0 are presented in Fig. S1 (Supporting Information). The sorption kinetics of Pb on the three SBCs were expressed well by the pseudo-second-order model, rather than pseudo-first-order model, which was indicated by their respective r^2 values (Table S1). About three hours was required for Pb sorption on the three BCs to reach the equilibrium likely through predominant chemisorption processes (Lu et al., 2012; Bandara et al., 2020).

The sorption isotherms of Pb on BC-N and BC-H were interpreted by the Langmuir model with r^2 values of 0.981 and 0.920, respectively (Table S2, Fig. 2). Fitting of sorption data to the Langmuir model indicated that the Pb sorption on BC-N and BC-H occurred mainly through surface monolayer interactions (Wu et al., 2017). However, the Freundlich model provided a better fit than the Langmuir model for BC-L with a r^2 value of 0.925 (Table S2, Fig. 2), which indicated that the Pb sorption on BC-L was predominated by a multilayer sorption process (Xia et al., 2019).

The maximum Langmuir sorption capacity values of Pb on BC-N, BC-L and BC-H under the same experimental conditions were 75.6, 46.0 and 91.3 mg g^{-1}, respectively. Only a few previous studies reported the

sorption of Pb on SBC. Wang et al. (2011) showed that the wheat-residue derived BC could sorb Pb up to 0.65 mmol g^{-1} (equal to 134 mg g^{-1}) at Pb concentration of 20 mmol L^{-1}. The sorption capacity of wheat-residue derived BC was higher than that of the three SBCs in this study. However, the maximum amount of Pb sorption to biochar (artificial BC) produced from different agricultural biomass might range from 13.1 to 88.7 mg g^{-1} (Table S3). Unraveling the sorption mechanisms of Pb to different SBCs can help to understand the difference in the sorption capacities of SBCs for Pb. The exact Pb fractions on Pb-loaded SBCs would be able to reveal the related sorption mechanisms of Pb to SBCs.

In the desorption experiments, the total Pb amount (Q_{tot}) and Pb amount of four sorbed fractions, e.g., physical sorption (Q_{phy}), ion exchange (Q_{exc}), hydrogen bonding (Q_{hyd}) and complexation (Q_{com}) fractions are shown in Fig. 3. With the increase of initial concentration of Pb, the amount of Pb in Q_{phy}, Q_{com}, Q_{hyd}, and Q_{exc} fractions reached the sorption equilibrium successively, indicating that the exact saturation order of the four Pb fractions was Q_{phy}, Q_{com}, Q_{hyd}, and Q_{exc}. The Q_{exc}, Q_{hyd}, Q_{com} and Q_{tot} on the three types of Pb-loaded SBCs were all found to be well fitted to the Langmuir model (Table S4) with high r^2 values ranging from 0.971 to 0.987, which was attributed to the fact that Pb desorption from Pb-loaded SBCs was a reverse process on Pb sorption to SBCs (Andreas and Zhang, 2014).

The percentage of sorbed Pb in Q_{hyd} and Q_{com} fractions of Pb-loaded SBCs (at Pb concentration of 1000 mg L^{-1}) significantly decreased from 48.9 and 20.1% to 43.4 and 12.7% under no-cultivation in comparison to the low cultivation intensity, while decreased to 43.0 and 13.1% under high cultivation intensity (Fig. 4). The percentage of Pb in the Q_{exc} fraction on SBCs however increased from 26.8% to 35.1 and 39.0%, respectively, from no-cultivation to low and high cultivation intensities. Results showed that Q_{exc} and Q_{hyd} were the two most important Pb fractions on the three Pb-loaded SBCs. The sum of Pb amounts in Q_{exc} and Q_{hyd} of the three Pb-loaded SBCs was ranging from 35.2 to 56.1 mg g^{-1}, and accounting for 75.7 to 82.0% of total sorbed Pb

(Table S5 and Fig. 4). Previous research also reported that biochar could remove metal ions from aqueous solutions by various mechanisms including electrostatic attraction, complex formation, reduction and precipitation (Lu et al., 2012; Li et al., 2019b). Similarly, Andreas and Zhang (2014) reported that metal sorption onto soil-derived humin (a specific organic matter) in freshwater media was dominated by hydrogen bonding and ion exchange fractions.

The content of BC-N, BC-L and BC-H in the soils was 2.85, 5.69 and 4.07 g kg^{-1}, while Pb amount in the Q_{com} fraction of these Pb-loaded SBCs was 11.52, 5.68 and 8.95 mg g^{-1}, respectively (Table S5 and Fig. 4). The complexation (Q_{com}) fraction of Pb was presented to be stable since the extracting agents such as ultrapure water, CH_3COONH_4 (1 M, pH=7), CH_3COOH (4.37 M) and $NH_2OH{\cdot}HCl$ (0.04 M) could not extract this Pb fraction (Andreas and Zhang, 2014) from the Pb-loaded SBCs. Therefore, we inferred that the BC-N, BC-L and BC-H might increase the capacity of Soil 1, Soil 2 and Soil 3 to adsorb Pb as a stable (complexation) fraction by 19.0, 18.7 and 21.1 mg kg^{-1} (Table S5), respectively.

3.3. Sorption mechanisms of Pb to SBCs

It was reported that the efficacy of various biochars derived from different biomass materials to adsorb PTE contaminants depends on its properties, e.g., surface area, pore size distribution, ion-exchange capacity (Bandara et al., 2020) and surface oxygen-containing functional groups (Xia et al., 2019) representing different sorption mechanisms. Accordingly, the sorption mechanisms of Pb onto SBCs were divided into the following four parts.

(1) Physical sorption: The orders of Q_{phy} on Pb-loaded SBCs and SSA of SBCs were both in the order: BC-L > BC-H > BC-N (Table S5 and Table 1), while the SSA values of SBCs was highly correlated to Q_{phy} fractions on Pb-loaded SBCs with a correlation coefficient (R^2) value of 0.94 (Fig. S2a). Similar results were reported by Zhang et al. (2019) who realized that the surface area of a sludge-based biochar was improved after

activation by different activators, thus improving its physical Pb sorption capacity. Moreover, Ngambia et al. (2019) found that tunnels on the rods of sludge derived carbon provided a high surface area, extra sorption sites and interspace for easy contamination diffusion contributing to surface physical adsorption.

(2) Ion exchange: The CEC values of SBCs were highly correlated to the Q_{exe} fractions of Pb-loaded SBCs with a correlation coefficient (R^2) of 0.833 (Fig. S2b). Moreover, the CEC values of SBCs and Q_{exe} fractions of Pb on Pb-loaded SBCs all followed the order: BC-H > BC-L > BC-N (Table S5 and Table 1). Therefore, the Q_{exe} fraction of Pb-loaded SBCs might be mainly attributed to the cation exchange mechanism of Pb sorption on SBCs.

The sum amounts of Na^+, K^+, Mg^{2+} and Ca^{2+} released in the supernatants after Pb sorption onto BC-N, BC-L and BC-H were equivalent to 13.3, 15.6 and 18.6 mg Pb g^{-1}, accounting for 23.1, 34.9 and 27.2% of the total Pb sorbed by BC-N, BC-L and BC-H (prepared under Pb concentration of 1000 mg L^{-1}), respectively (Table S6). The sum amounts of Na^+ and K^+ (mono-valent cations), which could be related to the electrostatic ion exchange with Pb (Lu et al., 2012) since they cannot form precipitates or be coordinated with surface functional groups of BCs, were equivalent to 5.32, 3.0 and 3.67 mg Pb g^{-1} accounting for 34.5, 19.1 and 13.8% of the Q_{exc} values on Pb-loaded BC-N, BC-L and BC-H, respectively (Table S6). Meanwhile, the sum amounts of Mg^{2+} and Ca^{2+} (divalent alkaline earth cations), which could originate from the exchange sites of inorganic minerals and the chelated surface functional groups such as R-COO−Me or R−O−Me on SBCs, were equivalent to 7.95, 12.6 and 15.0 mg Pb g^{-1} accounting for 51.6, 80.2 and 56.1% of the Q_{exc}, respectively (Table S6). Our results showed that the exchange sites adsorbed or chelated Pb fractions in Q_{exc} of Pb-loaded SBCs were far more than that of the electrostatically ion exchanged Pb fraction, indicating that chelation might have played a more important role during the sorption process (Lu et al., 2012). Similar result was reported by Li et al. (2019b) that ion exchange was the main mechanism for Pb sorption by coconut-fiber biochar with electrostatic ion exchange and chelation

processes.

(3) Hydrogen bonding: The results of TG and DTG thermograms of the three SBCs are shown in Fig. S3. The TG and DTG analyses detected three endothermic peaks between 30 and 180 °C, 300 and 350 °C, and 380 and 560 °C for all samples (Fig. S3). Previous studies ascribed the endothermic peak at temperatures below 200 °C to the loss of adsorbed water, while that near 325 °C to decarboxylation (volatilization of −COOH) and further dehydroxylation (volatilization of −OH) of surface organic functional groups, and that around 475 °C to the thermal reaction of the aromatic nuclei of organic matter (Plante et al., 2009). Carbohydrates and other aliphatic compounds would be pyrolyzed at 300 to 350 °C in the TG analysis (Plante et al., 2009), the weight loss of SBCs (Fig. S3; attributed to volatilization of −COOH and −OH), however, were highly correlated to the sum content of AOH and RCOOH groups (Table 1) with a R^2 value of 0.966 (Fig. S2c).

Moreover, the sum contents of AOH and RCOOH of SBCs were significantly correlated with Pb amount in the Q_{hyd} fraction (with a R^2 value of 0.833; Fig. S2d). This might be attributed to the activities of −COOH and −OH groups to adsorb Pb in aqueous solution through hydrogen bonding. It was reported that Pb would be present mainly as the species of Pb^{2+} at pH 4 in aqueous solution, then the amount of Pb^{2+} would decrease with an increase of pH to 5.5 due to $Pb(OH)^+$ formation (Ucun et al., 2003). Ucun et al. (2003) observed Pb precipitation ($Pb(OH)_2$) when the initial pH of a biosorption medium was adjusted to pH 5.5. Thus, Pb^{2+} and $Pb(OH)^+$ were likely to be adsorbed onto SBCs through hydrogen bonding at pH 5.0 as the Q_{hyd} fraction in this study.

(4) Complexation: In order to elucidate the complexation mechanism, the XPS spectra of C and O groups on the surface of SBCs with and without Pb loading were obtained for C 1s, O 1s and Pb 4f regions, and the corresponding changes in the functional groups were determined (Fig. 5 and Table 2). The peak at the binding energy of Pb 4f between 138 and 143 eV was found in all Pb-loaded SBC samples (Fig. 5b), which confirmed

388 that Pb was successfully complexed by the functional groups on SBCs. The binding energy of Pb 4f5/2 and
389 4f7/2 on Pb-loaded SBCs decreased to 143.79 eV and 138.89 eV in comparison with $Pb(NO_3)_2$ that centered at
390 145.0 eV and 139.9 eV (Batrusaitis et al., 2012; Xin et al., 2012), respectively, indicating the presence of strong
391 affinity between SBC and Pb ions by newly formed Pb−O groups (Zhang et al., 2017).

392 As shown in Fig. 5c−h, three principal C species, i.e., C−C/C=C/C−H (hydrocarbon) at 284.7 eV, C−O
393 (aromatic) at 286.4 eV and C=O/O−C=O (carboxylic carbon) at 288.4 eV, and two O species such as C−O at
394 531.9 eV and C=O at 532.8 eV were identified in the three SBC samples (Deng et al. 2017; Xia et al., 2019). After
395 Pb sorption, the peak intensities of C−O (aromatic) significantly decreased, while that of O=C−O (carboxylic
396 carbon) and C=O significantly increased (Table 2). These results indicated that O=C−O groups played key roles
397 in Pb sorption by forming complexes of O=C−O−Pb and/or O=C−O−Pb−O (Yamada et al., 2014; Wang et al.,
398 2015).

399 Overall, the above four mechanisms all likely attributed to Pb sorption onto SBCs, while they had various
400 degrees of contributions. However, the amount of Pb adsorbed onto SBCs was dominated by the ion exchange,
401 hydrogen bonding and complexation fractions. The amount of Pb in the physical sorption, ion exchange and
402 hydrogen bonding fractions on Pb-loaded SBCs were highly correlated with SSA, CEC and the sum contents of
403 hydroxyl and carboxyl functional groups on SBCs, respectively.

404

405 **4. Conclusions**

406 The amount of Pb adsorbed onto different SBCs was dominated by the ion exchange and hydrogen bonded
407 fractions, which together accounted for about 80% of the total sorbed Pb, and was mainly attributed to CEC and
408 hydrogen bonding capacities of free carboxyl and hydroxyl groups of SBCs. The increased cultivation intensity
409 and aging of SBCs increased the H/C, O/C ratios and CEC of the SBCs compared to that with no cultivation.

Therefore, the Pb sorption capacity of SBCs in the ion exchange fraction increased with the increasing cultivation intensity of soils. The maximum Pb sorption capacities of SBCs in this study were as high as that of biochars produced from various agricultural biomasses. Moreover, the SBCs might increase the Pb sorption capacities of the studied soils by 18.7 - 21.1 mg kg^{-1} in stable fractions, which might not be released readily. Overall, SBCs in soils under all studied cultivation intensities showed high potential to sorb and retain Pb in a stable form. Increasing SBC content in soil during land management and utilization could befittingly be an environment-friendly method to enhance the potential Pb immobilization capacity of soils. Further research should be carried out to determine the PTE sorption capacity of SBCs in ecologically and climatically different soils, so as to establish a database of PTE immobilization capacity of SBCs in soils.

Acknowledgements

This work was financially supported by the National Key Research and Development Program of China (2017YFD0202101), the National Natural Science Foundation of China (21866013, 21876027), the United Fund of Guangdong Provincial Basic and Applied Basic Research Foundation, China (2019A1515110705), the Crop Science Postgraduate Innovation Project of Hainan University Tropical Agriculture and Forestry College, China (ZWCX2018012, ZWCX2018013), and the Special Fund for the Science and Technology Innovation Team of Foshan, China (1920001000083).

References

Ali, S., Rizwan, M., Shakoor, M.B., Jilani, A., Anjum, R., 2020. High sorption efficiency for As(III) and As(V) from aqueous solutions using novel almond shell biochar, Chemosphere. 243, 125330. https://doi.org/10.1016/j.chemosphere.2019.125330

Andreas, R., Zhang, J., 2014. Characteristics of adsorption interactions of cadmium(II) onto humin from peat soil in freshwater and seawater media. B. Environ. Contam. Tox. 92, 352–357. https://doi.org/10.1007/s00128-014-1205-x

Bandara, T., Franks, A., Xu, J., Bolan, N., Wang, H., Tang, C., 2020. Chemical and biological immobilization mechanisms of potentially toxic elements in biochar-amended soils. Crit. Rev. Environ. Sci. Technol. 50, 903-978. doi:10.1080/10643389.2019.1642832

Bao, S., 2000. Chemical Analysis for Agricultural Soil. China Agriculture Press, Beijing.

Batrusaitis, J., Chen, H.H., Rubasinghege, G., Grassian, V.H., 2012. Heterogeneous atmospheric chemistry of lead oxide particles with nitrogen dioxide increases lead solubility: environmental and health implications. Environ. Sci. Technol. 46 (23), 12806–12813. https://doi.org/10.1021/es3019572

Bennett, L.T., Hinko-Najera, N., Aponte, C., Nitschke, C.R., Fairman, T.A., Fedrigo, M., Kasel, S., 2020. Refining benchmarks for soil organic carbon in Australia's temperate forests. Geoderma 368, 11424. https://doi.org/10.1016/j.geoderma.2020.114246

Boehm, H.P., 1994. Some aspects of the surface chemistry of carbon blacks and other carbons. Carbon 32 (5), 759–769. https://doi.org/10.1016/0008-6223(94)90031-0

Brunauer, S., Emmett, P.H., Teller, E., 1938. Adsorption of gases in multimolecular layers. J. Am. Chem. Soc. 60 (2), 309–319. https://doi.org/10.1021/ja01269a023

Cao, Y., Jing, Y., Hao, H., Wang, X., 2019. Changes in the physicochemical characteristics of peanut straw biochar after freeze-thaw and dry-wet aging treatments of the biomass. BioResources 14(2), 4329–4343. https://doi.org/10.15376/biores.14.2.4329-4343

Chen, H., Yang, X., Wang, H., Sarkar, B., Shaheen, S.M., Gielen, G., Bolan, N., Guo, J., Che, L., Sun, H., Rinklebe, J., 2020a. Animal carcass- and wood-derived biochars improved nutrient bioavailability, enzyme activity, and plant growth in metal-phthalic acid ester co-contaminated soils: A trial for reclamation and improvement of degraded soils. Journal of

Environmental Management 261, 110246. https://doi.org/10.1016/j.jenvman.2020.110246

Chen, Y., Lee, S., Tahmasebi, A., Bai, J., Vongsvivut, J., Yu, J., 2020b. Chemical structure transformation during the later stage of plastic layers during coking using Synchrotron infrared microspectroscopy technique. Fuel. 273, 117764. https://doi.org/10.1016/j.fuel.2020.117764

Cheng, C.-H., Lehmann, J., Engelhard, M.H., 2008. Natural oxidation of black carbon in soils: Changes in molecular form and surface charge along a climosequence. Geochim. Cosmochim. Ac. 72, 1598–1610. https://doi.org/10.1016/j.gca.2008.01.010

Chiou, C.T., 2002. Partition and Adsorption of Organic Contaminants in Environmental Systems. Wiley-Interscience. https://doi.org/10.1016/S0304-3894(02)00361-8

D1762-84, 2007. Standard Test Method for Chemical Analysis of Wood Charcoal. American Society for Testing and Materials, Conshohocken, PA.

Deng, J., Liu, Y., Liu, S., Zeng, G., Tan, X., Huang, B., Tang, X., Wang, S., Hua, Q., Yan, Z., 2017. Competitive adsorption of Pb(II), Cd(II) and Cu(II) onto chitosan-pyromellitic dianhydride modified biochar. J. Colloid. Interface. Sci. 506, 355–364. https://doi.org/10.1016/j.jcis.2017.07.069

Dodson, J., Li, J., Lu, F., Zhang, W., Yan, H., Cao, S., 2019. A late pleistocene and holocene vegetation and environmental record from shuangchi maar, hainan province, South China. Palaeogeogr. Palaeocl. 523, 89–96. https://doi.org/10.1016/j.palaeo.2019.03.026

Dong, X., Li, G., Lin, Q., Zhao, X., 2017. Quantity and quality changes of biochar aged for 5 years in soil under field conditions. Catena 159, 136–143. https://doi.org/10.1016/j.catena.2017.08.008

Fang, Z., Gao, Y., Bolan, N., Shaheen, S.M., Xu, S., Wu, X., Xu, X., Hu, H., Lin, J., Zhang, F., Li, J., Rinklebe, J., Wang, H., 2020. Conversion of biological solid waste to graphene-containing biochar for water remediation: A critical review. Chem. Eng. J. 390, 124611. https://doi.org/10.1016/j.cej.2020.124611

476 Hardy, B., Leifeld, J., Knicker, H., Dufey, J.E., Deforce, K., Cornélis, J.T., 2017. Long term change in chemical properties of
477 preindustrial charcoal particles aged in forest and agricultural temperate soil. Org. Geochem. 107, 33–45.
478 https://doi.org/10.1016/j.orggeochem.2017.02.008
479 Imran, M., Khan, Z.U.H., Iqbal, J., Shah, N.S., Muzammil, S., Ali, S., Muhammad, N., Aziz, A., Murtaza, B., Naeem, M.A.,
480 Amjad, M., Shahid, M., Zakir, A., Rizwan, M., 2020. Potential of siltstone and its composites with biochar and
481 magnetite nanoparticles for the removal of cadmium from contaminated aqueous solutions: Batch and column scale
482 studies, Environ. Pollut. 259, 113938. https://doi.org/10.1016/j.envpol.2020.113938
483 Jaffé, R., Ding, Y., Niggemann, J., Vähätalo, A. V, Stubbins, A., Spencer, R.G.M., Campbell, J., Dittmar, T., 2013. Global
484 charcoal mobilization from soils via dissolution and riverine transport to the oceans. Science 340, 345–347.
485 https://doi:10.1126/science.1231476
486 Koide, R. T., Petprakob, K., Peoples, M., 2011. Quantitative analysis of biochar in field soil. Soil Biol. Biochem. 43,
487 1563–1568. https://doi.org/10.1016/j.soilbio.2011.04.006
488 Lehmann, J., Liang, B., Solomon, D., Lerotic, M., Luizão, F., Kinyangi, J., Schäfer, T., Wirick, S., Jacobsen, C., 2005.
489 Near-edge X-ray absorption fine structure (NEXAFS) spectroscopy for mapping nano-scale distribution of organic
490 carbon forms in soil: Application to carbon particles. Global. Biogeochem. Cy. 19,
491 https://doi.org/10.1029/2004GB002435
492 Li, J., Wang, S.-L., Zhang, J., Zheng, L., Chen, D., Wu, Z., Shaheen, S.M., Rinklebe, J., Ok, Y.S., Wang, H., Wu, W., 2020.
493 Coconut-fiber biochar reduced the bioavailability of lead but increased its translocation rate in rice plants: Elucidation
494 of immobilization mechanisms and significance of iron plaque barrier on roots using spectroscopic techniques. J.
495 Hazard. Mater. 389, 122117. https://doi.org/10.1016/j.jhazmat.2020.122117
496 Li, J., Wang, S.-L., Zheng, L., Chen, D., Wu, Z., Xie, Y., Wu, W., Niazi, N.K., Ok, Y.S., Rinklebe, J., Wang, H., 2019a.
497 Sorption of lead in soil amended with coconut fiber biochar: Geochemical and spectroscopic investigations. Geoderma

350, 52–60. https://doi.org/10.1016/j.geoderma.2019.05.008

Li, J., Zheng, L., Wang, S.-L., Wu, Z., Wu, W., Niazi, N.K., Shaheen, S.M., Rinklebe, J., Bolan, N., Ok, Y.S. Wang, H., 2019b. Sorption mechanisms of lead on silicon-rich biochar in aqueous solution: Spectroscopic investigation. Sci. Total Environ. 672, 572–582. https://doi.org/10.1016/j.scitotenv.2019.04.003

Liang, B., Lehmann, J., Solomon, D., Kinyangi, J., Grossman, J., O'Neill, B., Skjemstad, J. O., Thies, J., Luizão, F. J., Petersen, J., 2006. Black carbon increases cation exchange capacity in soil. Soil. Sci. Soc. Am. J. 70, 1719–1730. https://doi.org/10.2136/sssaj2005.0383

Liang, B., Lehmann, J., Solomon, D., Sohi, S., Thies, J. E., Skjemstad, J. O., Luizão, F. J., Engelhard, M. H., Neves, E. G., Wirick, S., 2008. Stability of biomass-derived black carbon in soils. Geochim. Cosmochim. Ac. 72, 6069–6078. https://doi.org/10.1016/j.gca.2008.09.028

Liu, H., Xu, F., Xie, Y., Wang, C., Zhang, A., Li, L., Xu, H., 2018. Effect of modified coconut shell biochar on availability of heavy metals and biochemical characteristics of soil in multiple heavy metals contaminated soil. Sci. Total Environ. 645, 702–709. https://doi.org/10.1016/j.scitotenv.2018.07.115

Lu, H., Zhang, W., Yang, Y., Huang, X., Wang, S., Qiu, R., 2012. Relative distribution of Pb^{2+} sorption mechanisms by sludge-derived biochar. Water. Res. 46, 854–862. https://doi.org/10.1016/j.watres.2011.11.058.

Lu, K., Yang, X., Gielen, G., Bolan, N., Ok, Y.S., Niazi, N.K., Xu, S., Yuan, G., Chen, X., Zhang, X., Liu, D., Song, Z., Liu, X., Wang, H., 2017. Effect of bamboo and rice straw biochars on the mobility and redistribution of heavy metals (Cd, Cu, Pb and Zn) in contaminated soil. J. Environ.Manag. 186, 285–292. https://doi.org/10.1016/j.jenvman.2016.05.068.

Lu, X., Zang, R., Ding, Y., Huang, J., 2018. Partitioning the functional variation of tree seedlings during secondary succession in a tropical lowland rainforest. Ecosphere 9(6), e02305. https://doi.org/10.1002/ecs2.2305

Mia, S., Dijkstra, F.A., Singh, B., 2017. Chapter one – long-term aging of biochar: a molecular understanding with agricultural and environmental implications. Adv. Agron. 141, 1–51. https://doi.org/10.1016/bs.agron.2016.10.001

Mukherjee, A., Zimmerman, A.R., Cooper, W.T., Hamdan, R., 2014. Physicochemical changes in pyrogenic organic matter (biochar) after 15 months of field aging. Solid Earth 5(2), 693–704. https://doi.org/10.5194/se-5-693-2014

Mumtaz, I., Majeed, Z., Ajab, Z., Ahmad, B., Khurshid, K., Mubashir, M., 2019. Optimized tuning of rosin adduct with maleic anhydride for smart applications in controlled and targeted delivery of urea for higher plant's uptake and growth efficiency. Ind. Crop. Prod. 133, 395–408. https://doi.org/10.1016/j.indcrop.2019.02.036

Ngambia, A., Ifthikar, J., Shahib, I. I., Jawad, A., Shahzad, A., Zhao, M., Wang, J., Chen, Z., Chen, Z., 2019. Adsorptive purification of heavy metal contaminated wastewater with sewage sludge derived carbon-supported Mg(II) composite. Sci. Total Environ. 691, 306–321. https://doi.org/10.1016/j.scitotenv.2019.07.003

Nie, C., Yang, X., Niazi, N.K., Xu, X., Wen, Y., Rinklebe, J., Ok, Y.S., Xu, S., Wang, H., 2018. Impact of sugarcane bagasse-derived biochar on heavy metal availability and microbial activity: A field study. Chemosphere 200, 274-282.https://doi.org/10.1016/j.chemosphere.2018.02.134

Nolan, R.H., Boer, M.M., Collins, L., Resco de Dios, V., Clarke, H., Jenkins, M., Kenny, B., Bradstock, R.A., 2020. Causes and consequences of eastern Australia's 2019–20 season of mega-fires. Global Change Biol. 26(3), 1039–1041. https://doi.org/10.1111/GCB.14987

Pereira, R.C., Arbestain, M.C., Kaal, J., Sueiro, M.V., Sevilla, M., Hindmarsh, J., 2014. Detailed carbon chemistry in charcoals from pre-European Maori gardens of New Zealand as a tool for understanding biochar stability in soils. Eur. J. Soil Sci. 65, 83–95. https://doi.org/10.1111/ejss.12096

Plante, A. F., Fernández, J. M., Leifeld, J., 2009. Application of thermal analysis techniques in soil science. Geoderma 153(1–2), 1–10. https://doi.org/10.1016/j.geoderma.2009.08.016

Qi, F.J., Kuppusamy, S., Naidu, R., Bolan, N.S., Ok, Y.S., Lamb, D., Li, Y.B., Yu, L.B., Semple, K.T., Wang, H.L., 2017. Pyrogenic carbon and its role in contaminant immobilization in soils. Critical Reviews in Environmental Science and Technology 47, 795-876. doi:10.1080/10643389.2017.1328918

Qin, P., Wang, H., Yang, X., He, L., Müller, K., Shaheen, S.M., Xu, S., Rinklebe, J., Tsang, D.C.W., Ok, Y.S., Bolan, N., Song, Z., Che, L., Xu, X., 2018. Bamboo- and pig-derived biochars reduce leaching losses of dibutyl phthalate, cadmium, and lead from co-contaminated soils. Chemosphere 198, 450-459. https://doi.org/10.1016/j.chemosphere.2018.01.162

Schmidt, M.W.I., Noack, A.G., 2000. Black carbon in soils and sediments: Analysis, distribution, implications, and current challenges. Global Biogeochem. Cy. 14, 777–793. https://doi.org/10.1029/1999GB001208

Ucun, H., Bayhana, Y.K., Kaya, Y., Cakici, A., Algur, O.F., 2003. Biosorption of lead (II) from aqueous solution by cone biomass of Pinus sylvestris. Desalination 154, 233–238. https://doi.org/10.1016/s0011-9164(03)80038-3

Wang, C., Liu, J., Shen, J., Chen, D., Li, Y., Jiang, B., Wu, J., 2018. Effects of biochar amendment on net greenhouse gas emissions and soil fertility in a double rice cropping system: a 4-year field experiment. Agr. Ecosyst. Environ. 262, 83−96. https://doi.org/10.1016/j.agee.2018.04.017

Wang, H., Gao, B., Wang, S., Fang, J., Xue, Y., Kai, Y., 2015. Removal of Pb(II), Cu(II), and Cd(II) from aqueous solutions by biochar derived from $KMnO_4$ treated hickory wood. Bioresour. Technol. 197, 356–362. https://doi.org/10.1016/j.biortech.2015.08.132

Wang, J., Ren, C., Cheng, H., Zou, Y., Bughio, M. A., Li, Q., 2017a. Conversion of rainforest into agroforestry and monoculture plantation in China: consequences for soil phosphorus forms and microbial community. Sci. Total Environ. 595, 769–778. https://doi.org/10.1016/j.scitotenv.2017.04.012

Wang, L., Wang, Y., Ma, F., Tankpa, V., Bai, S., Guo, X., Wang, X., 2019. Mechanisms and reutilization of modified biochar used for removal of heavy metals from wastewater: A review. Sci. Total Environ. 668, 1298–1309. https://doi.org/10.1016/j.scitotenv.2019.03.011

Wang, X., Miao, H., He, W., Shen, H., 2011. Competitive adsorption of Pb(II), Cu(II), and Cd(II) ions on wheat-residue derived black carbon. J. Chem. Eng. Data 56(3), 444–449. https://doi.org/10.1021/je101079w

564 Wei, J., Tu, C., Yuan, G., Zhou, Y., Wang, H., Lu, J., 2020. Limited Cu(II) binding to biochar DOM: Evidence from C K-edge
565 NEXAFS and EEM-PARAFAC combined with two-dimensional correlation analysis. Science of The Total
566 Environment 701, 134919. https://doi.org/10.1016/j.scitotenv.2019.134919
567 Wu, W., Li, J., Lan, T., Müller, K., Niazi, N. K., Chen, X., Xu, S., Zheng, L., Chu, Y., Li, J., 2017. Unraveling sorption of
568 lead in aqueous solutions by chemically modified biochar derived from coconut fiber: A microscopic and spectroscopic
569 investigation. Sci. Total Environ. 576, 766–774. https://doi.org/10.1016/j.scitotenv.2016.10.163.
570 Wu, W., Li, J., Niazi, N. K., Müller, K., Chu, Y., Zhang, L., Yuan, G., Lu, K., Song, Z., Wang, H., 2016. Influence of
571 pyrolysis temperature on lead immobilization by chemically modified coconut fiber-derived biochars in aqueous
572 environments. Environ. Sci. Pollut. Res. 23, 22890–22896. https://doi.org/10.1007/s11356-016-7428-0.
573 Wu, W., Yang, M., Feng, Q., McGrouther, K., Wang, H., Lu, H.H., Chen, Y.X., 2012. Chemical characterization of rice
574 straw-derived biochar for soil amendment. Biomass Bioenergy 47, 268–276.
575 https://doi.org/10.1016/j.biombioe.2012.09.034.
576 Xia, Y., Yang, T., Zhu, N., Li, D., Chen, Z., Lang, Q., Liu, Z., Jiao, W., 2019. Enhanced adsorption of Pb (II) onto modified
577 hydrochar: modeling and mechanism analysis. Bioresour. Technol. 121593.
578 https://doi.org/10.1016/j.biortech.2019.121593
579 Xin, X., Qin, W., Jian, Y., Yan, L., Rui, F., Chen, G., Du, B., He, L., 2012. Highly efficient removal of heavy metal ions by
580 amine-functionalized mesoporous Fe_3O_4 nanoparticles. Chem. Eng. J. 184, 132–140.
581 https://doi.org/10.1016/j.cej.2012.01.016
582 Yamada, Y., Suzuki, Y., Yasuda, H., Uchizawa, S., Hirose-Takai, K., Sato, Y., Suenaga, K., Sato, S., 2014. Functionalized
583 graphene sheets coordinating metal cations. Carbon 75, 81−94. https://doi.org/10.1016/j.carbon.2014.03.036
584 Yang, X., Wan, Y., Zheng, Y., He, F., Yu, Z., Huang, J., Wang, H., Ok, Y.S., Jiang, Y., Gao, B., 2019. Surface functional
585 groups of carbon-based adsorbents and their roles in the removal of heavy metals from aqueous solutions: A critical

review. Chem. Eng. J. 366, 608–621. https://doi.org/10.1016/j.cej.2019.02.119

Yin, G., Song, X., Tao, L., Sarkar, B., Sarmah, A.K., Zhang, W., Lin, Q., Xiao, R., Liu, Q., Wang, H., 2020. Novel Fe-Mn binary oxide-biochar as an adsorbent for removing Cd(II) from aqueous solutions. Chemical Engineering Journal 389, 124465. https://doi.org/10.1016/j.cej.2020.124465

Zahedifar, M., 2017. Sequential extraction of zinc in the soils of different land use types as influenced by wheat straw derived biochar. J. Geochem. Explor. 182, 22–31. https://doi.org/10.1016/j.gexplo.2017.08.007

Zhang, J., Shao, J., Jin, Q., Li, Z., Zhang, X., Chen, Y., Zhang, S., Chen, H., 2019. Sludge-based biochar activation to enhance Pb (II) adsorption. Fuel 252, 101–108. https://doi.org/10.1016/j.fuel.2019.04.096

Zhang, M., Fellowes, J. R., Jiang, X., Wang, W., Chan, B. P. L., Ren, G. , Zhu, J. G., 2010. Degradation of tropical forest in Hainan, China, 1991-2008: conservation implications for hainan gibbon (nomascus hainanus). Biol. Conserv. 6(143), 1397–1404. https://doi.org/10.1016/j.biocon.2010.03.014

Zhang, Q., Yang, Q., Phanlavong, P., Li, Y., Peng, Q., 2017. Highly efficient lead(II) sequestration using size-controllable polydopamine microspheres with superior application capability and rapid capture. Acs Sustain. Chem. Eng. 5, 4161–4170. https://doi.org/10.1021/acssuschemeng.7b00129

Zhang, X., Gao, B., Fang, J., Zou, W., Dong, L., Cao, C., Zhang, J., Li, Y., Wang, H., 2019. Chemically activated hydrochar as an effective adsorbent for volatile organic compounds (VOCs). Chemosphere 218, 680-686. https://doi.org/10.1016/j.chemosphere.2018.11.144

Zhou, T., Wu, L., Luo, Y., Christie, P., 2018. Effects of organic matter fraction and compositional changes on distribution of cadmium and zinc in long-term polluted paddy soils. Environ. Pollut. 232, 1–9. https://doi.org/10.1016/j.envpol.2017.09.081

608 **Figure captions**

609 **Fig. 1.** The FTIR spectra of SBC samples.

610 **Fig. 2.** Isotherms of Pb sorption on SBCs.

611 **Fig. 3.** Total Pb amounts and Pb amounts of four fractions on the three Pb-loaded SBCs prepared under increasing initial

612 concentration of Pb.

613 **Fig. 4.** Amounts of Pb in different Pb fractions on Pb-loaded SBCs under Pb concentration of 1000 mg L^{-1}.

614 **Fig. 5.** XPS wide scan spectra of Pb 4f, C 1s and O 1s (a), high-resolution spectra of Pb 4f region (b), and high-resolution

615 spectra of C 1s regions (c–h) on SBCs before and after Pb sorption.

616

617

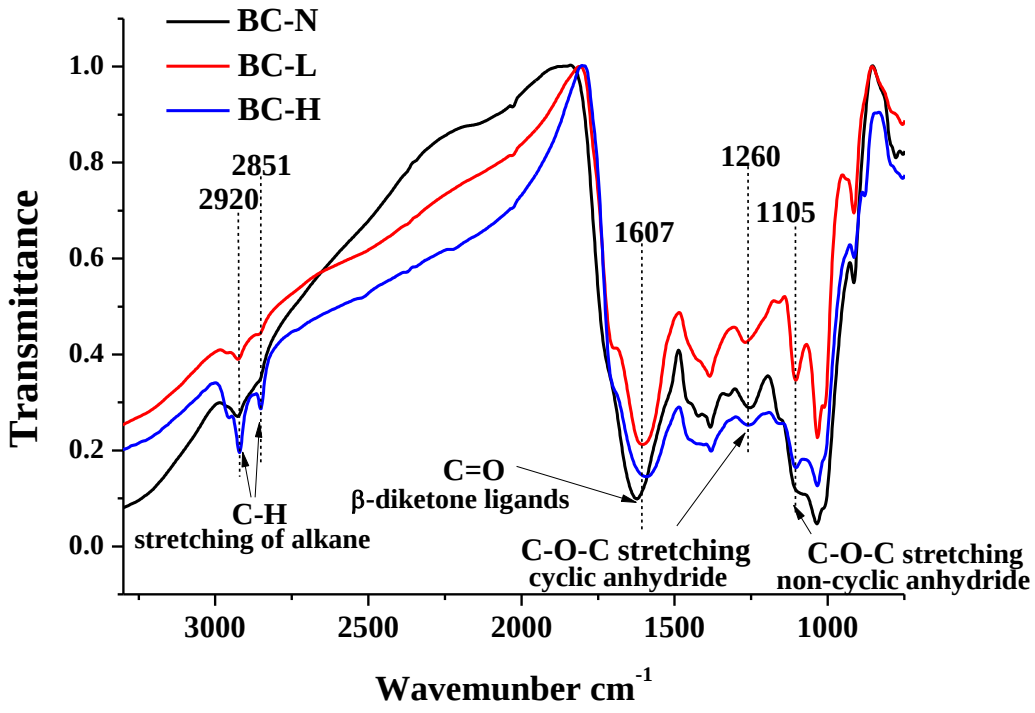

618

619 **Fig. 1.** The FTIR spectra of SBC samples, the sample ID of BC-N, BC-L and BC-H refer to SBC selected from Soil 1, Soil 2

620 and Soil 3, respectively.

621

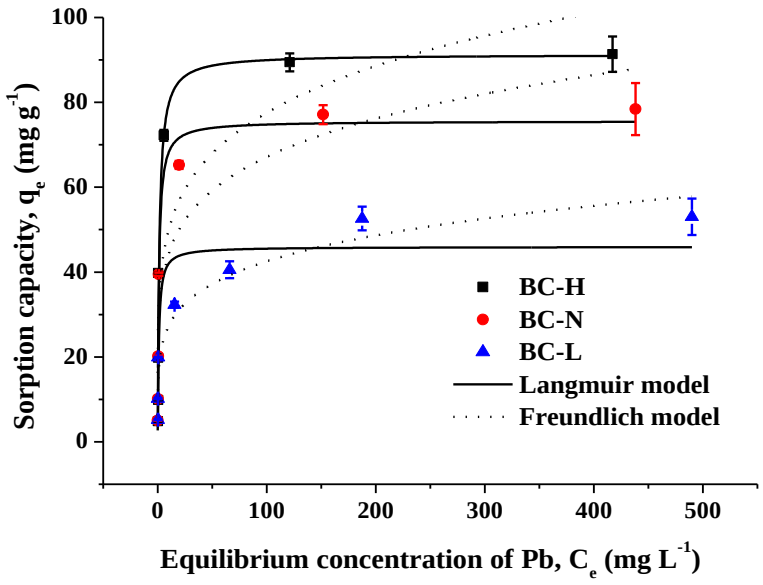

622

623 **Fig. 2.** Isotherms of Pb sorption on SBCs.

624

625

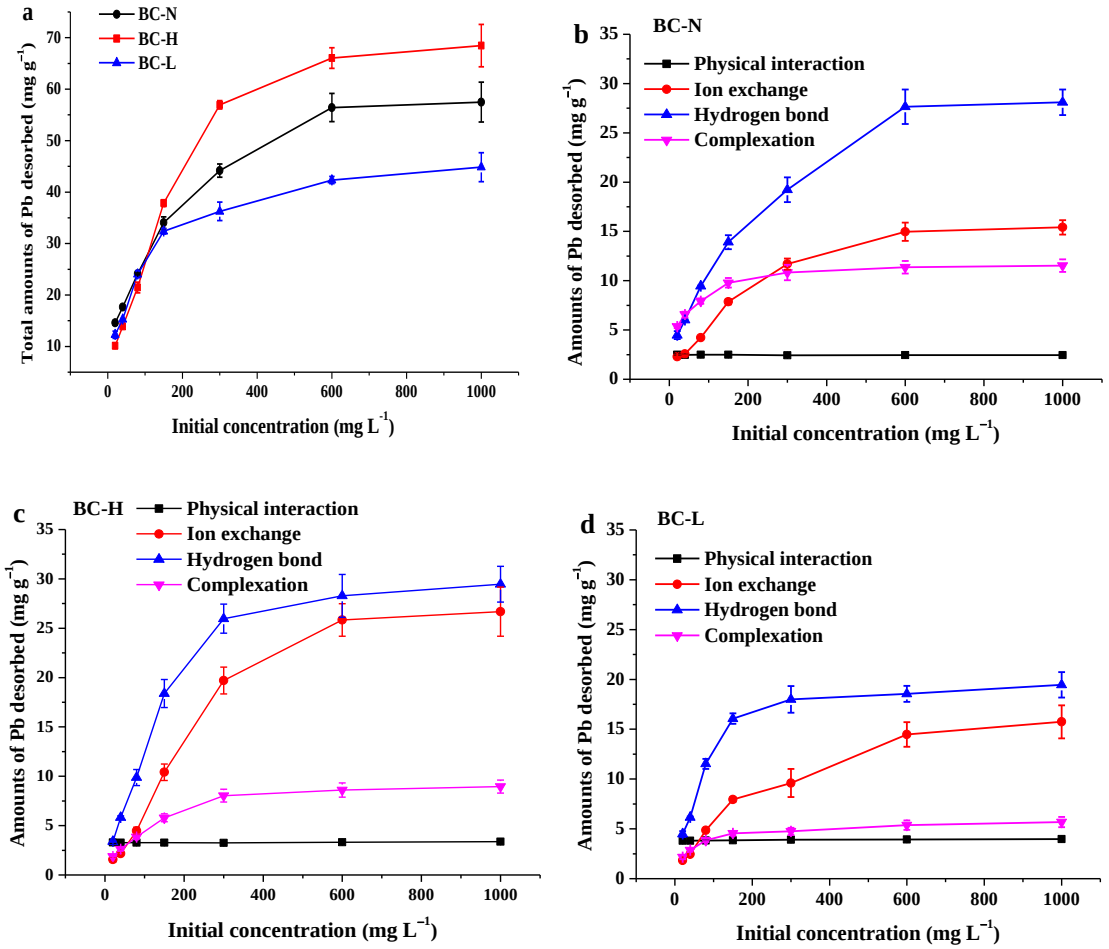

626

627 **Fig. 3.** Total Pb amounts and Pb amounts of four fractions on the three Pb-loaded SBCs prepared under increasing initial

628 concentration of Pb.

629

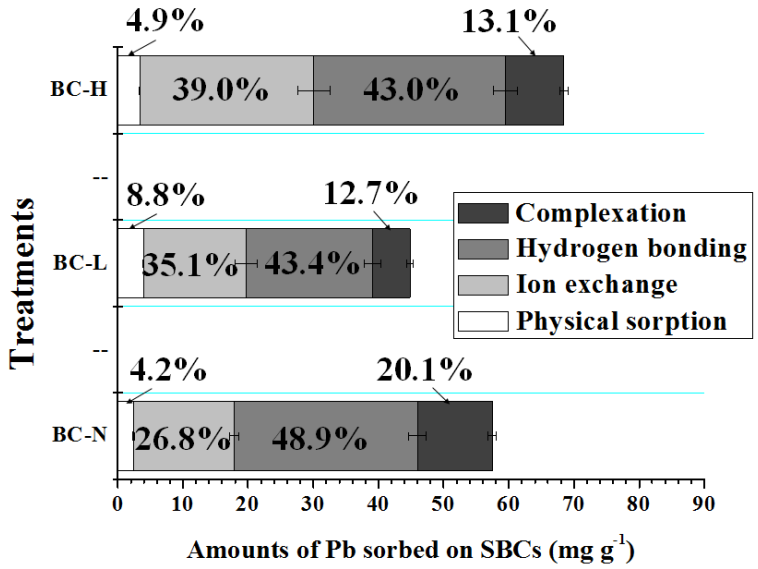

630

631 **Fig. 4.** Amounts of Pb in different Pb fractions on Pb-loaded SBCs under Pb concentration of 1000 mg L^{-1}.

632

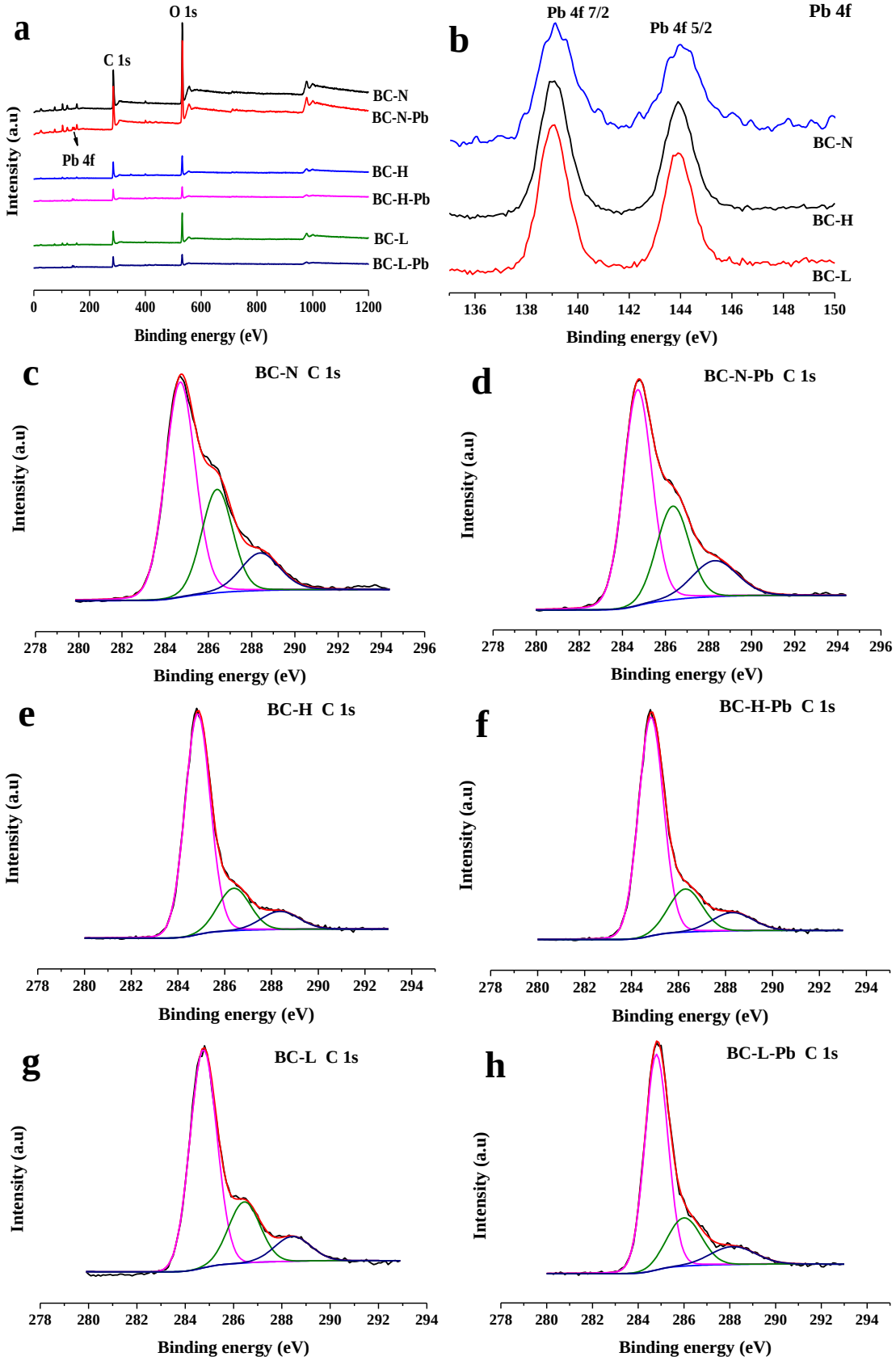

Fig. 5. XPS wide scan spectra of Pb 4f, C 1s and O 1s (a), high-resolution spectra of Pb 4f region (b), and high-resolution spectra of C 1s regions (c–h) on SBCs before and after Pb sorption.

Table 1. Composition and selected properties of SBCs.

Sample ID	Elemental component (%)				Atomic ratio			n(RCOOH)	n(RCOR')	n(AOH)	CEC	SSA (m^2 g^{-1})
	C	H	N	O	H/C	O/C	(O+N)/C	(mmol g^{-1})	(mmol g^{-1})	(mmol g^{-1})	(cmol kg^{-1})	
BC-N	49.1	3.61	0.73	46.5	0.88	0.71	0.72	0.53 ± 0.02	0.70 ± 0.03	0.34 ± 0.04	128.0 ± 24.9	7.51 ± 1.1
BC-L	47.9	3.87	1.64	46.6	0.97	0.73	0.76	0.49 ± 0.01	1.13 ± 0.19	0.09 ± 0.01	166.4 ± 13.4	34.1 ± 2.7
BC-H	45.9	3.90	2.36	47.8	1.02	0.78	0.83	0.03 ± 0.01	0.64 ± 0.03	1.03 ± 0.01	227.3 ± 11.7	20.3 ± 1.8

Notes: Results are means ± SD (n = 3), the sample ID of BC-N, BC-L and BC-H refer to SBC selected and picked from Soil 1 (no-cultivation), Soil 2 (less intensive cultivation) and Soil 3 (highly intensive cultivation), respectively. While the RCOOH, RCOR', and AOH refer to carboxylic acid, weak acid ester, and phenolic hydroxyl groups, respectively.

643 **Table 2.** Peak positions and relative contents of surface functional groups determined from C 1s and O 1s XPS spectra for
644 SBCs before and after Pb sorption.

Sample ID		Bonds and groups of C 1s			Bonds and groups of O 1s	
		C−C/C=C/C−H	C−O	C=O/O−C=O	C=O	C−O
BC-N	Beam energy (eV)	284.7	286.4	288.4	531.9	532.8
	Atomic percentage (%)	58.2	28.3	13.6	59.7	40.3
BC-N-Pb	Beam energy (eV)	284.7	286.3	288.3	532	532.8
	Atomic percentage (%)	57.4	27.5	15.1	62.3	37.7
BC-L	Beam energy (eV)	284.7	286.4	288.4	532	532.9
	Atomic percentage (%)	67.5	22.2	10.3	61.8	38.2
BC-L-Pb	Beam energy (eV)	284.7	286.3	288.3	531.8	532.8
	Atomic percentage (%)	67.7	21.8	10.5	62.4	37.6
BC-H	Beam energy (eV)	284.8	286.3	288.3	531.9	532.7
	Atomic percentage (%)	73.2	19.3	7.5	64.5	35.5
BC-H-Pb	Beam energy (eV)	284.8	286.3	288.3	531.9	533.2
	Atomic percentage (%)	72	18.5	9.5	77.4	22.6

645

646

Supplementary Material:

Sorption mechanisms of lead on soil-derived black carbon formed under varying cultivation systems

Qingjie Zhao [a,1], Jianhong Li [a,b,1], Binoy Sarkar [c], Weidong Wu [a], Boling Li [a], Ruichun Liu [d], Mohsin Nawaz [e], Muhammad Zia-ur-Rehman [f], Hailong Wang [b,g,], Zhipeng Wu [a,*]**

[a] College of Tropical Crops, Hainan University, Haikou 570228, China

[b] Biochar Engineering Technology Research Center of Guangdong Province, School of Environmental and Chemical Engineering, Foshan University, Foshan 528000, China

[c] Lancaster Environment Centre, Lancaster University, Lancaster, LA1 4YQ, United Kingdom

[d] Flood Control and Drought Relief Office of Hangjin County, Ordos 017400, China

[e] Key Laboratory of Genetics and Germplasm Innovation of Tropical Special Forest Trees and Ornamental Plants, Ministry of Education, College of Forestry, Hainan University, Haikou 570228, China

[f] Institute of Soil and Environmental Sciences, University of Agriculture, Faisalabad, 38040, Pakistan

[g] Key Laboratory of Soil Contamination Bioremediation of Zhejiang Province, Zhejiang A&F University, Hangzhou 311300, China

[*] Corresponding author.

[**] Correspondence to: H. Wang, School of Environmental and Chemical Engineering, Foshan University, Foshan 528000, China

E-mail addresses: hailong.wang@fosu.edu.cn (H. Wang), peter@hainanu.edu.cn (Z. Wu).

[1] Qingjie Zhao and Jianhong Li contributed to the work equally and should be considered co-first authors.

Text S1.

The pseudo-first-order (Eq. 1) and pseudo-second-order (Eq. 2) models used in this study:

$$\ln(q_e - q_t) = \ln q_e - k_1 t \quad (1)$$

$$t/q_t = 1/k_2 q_e^2 + 1/q_e \quad (2)$$

where, k_1 (h^{-1}) and k_2 ($h^{-1}\cdot(g\ mg^{-1})$) are the rate constants of the pseudo first-order and pseudo-second order models, respectively. While, q_e and q_t is the amount of Pb sorbed by SBC at equilibrium and at time (t) in mg g^{-1}, respectively.

The Langmuir (Eq. 3) and Freundlich (Eq. 4) models used in this study:

$$q_e = q_{max} K_L C_e / (1 + K_L C_e) \quad (3)$$

$$q_e = K_f C_e^{1/n} \quad (4)$$

where, q_e (mg g^{-1}) and C_e (mg L^{-1}) are the amounts of Pb sorbed by SBC for a given initial Pb concentration, and the concentration of Pb in solution at equilibrium, respectively. While, q_m (mg g^{-1}) is the maximum amount of Pb adsorbed at equilibrium, K_L (L mg^{-1}) is the Langmuir constant; n and K_f ((mg g^{-1})·(mg $L^{-1})^{-n}$) are equilibrium constants relating to sorption intensity and sorption capacity of the Freundlich model, respectively.

686 **Table S1.** Parameters of pseudo-first-order and pseudo-second-order kinetic models for Pb sorption on SBCs.

Sample ID	Pseudo-first-order			Pseudo-second-order		
	q_e (mg g^{-1})	k_1 (1 h^{-1})	r^2	q_e (mg g^{-1})	k_2 (g $mg^{-2}h^{-1}$)	r^2
BC-N	31.18	7.22	0.795	32.92	0.356	0.998
BC-L	27.33	0.89	0.787	30.66	0.034	0.979
BC-H	49.11	13.19	0.992	50.63	0.592	0.999

687

Table S2. Parameters of Langmuir and Freundlich isotherm models for Pb sorption on SBCs.

Sample ID	Langmuir			Freundlich		
	q_m (mg g^{-1})	K_L (L mg^{-1})	r^2	K_f (mg $^{(1-n)}$ L^n g^{-1})	n	r^2
BC-N	75.6	0.916	0.981	29.11	0.182	0.847
BC-L	46.0	1.064	0.854	17.53	0.193	0.925
BC-H	91.3	0.675	0.920	32.13	0.191	0.728

688

689

690 **Table S3.** Sorption capacities of different biochars for removing Pb from aqueous solution at pH of 5.0.

Type of biochars	Metal ion	Q_m (mg g^{-1})	References
Oak bark char	Pb^{2+}	13.1	Mohan et al. 2007
Pomelo peel biochar	Pb^{2+}	88.7	Zhao et al., 2018
Coconut-fiber biochar	Pb^{2+}	79.4	Li et al., 2019
Raw sugarcane bagasse biochar	Pb^{2+}	81.9	Inyang et al., 2011
Corn stover biochar	Pb^{2+}	63.3	Li et al., 2018
Digested sugar beet biochar	Pb^{2+}	51.4	Inyang et al., 2012

691

692 **Table S4.** The parameters (r^2) of Langmuir model for different Pb fractions on Pb-loaded SBCs under increasing
693 initial Pb concentrations.

Sample ID	Physical interaction	Ion exchange	Hydrogen bond	Complexation	Total amount
BC-N	-	0.984	0.983	0.971	0.969
BC-L	-	0.986	0.968	0.979	0.987
BC-H	-	0.966	0.973	0.984	0.983

694

Table S5. Amounts of Pb in different fractions on Pb-loaded SBCs (prepared under Pb concentration of 1000 mg L^{-1}).

Sample ID	Amount of Pb in different fractions (mg g^{-1})					Amount of sorbed Pb in a stable form in soil (mg kg^{-1})[α]
	Physical adsorption	Ion exchange	Hydrogen bonding	complexation	Total amount of desorption	
BC-N	2.44	15.41	28.10	11.53	57.48	19.0
BC-L	3.97	15.74	19.45	5.68	44.84	18.7
BC-H	3.37	26.68	29.46	8.95	68.46	21.1

[α]The amount of sorbed Pb in a stable form in soil (attribute to SBC sorption) was calculated by the equation: $Q_{sta} = M_{SBC} \times Q_{com}$, where Q_{sta}, M_{SBC}, and Q_{com} refer to the amount of stable Pb (in mg kg^{-1}), the content of SBC in soil (in g kg^{-1}), and amount of Pb in complexation fraction (in mg g^{-1}), respectively.

698 **Table S6.** Equivalents of adsorbed Pb by released cations from Pb-loaded SBCs.

Sample ID	K+ (mg g−1)	Na+ (mg g−1)	Ca2+ (mg g−1)	Mg2+ (mg g−1)
BC-N	1.32 ± 0.03	4.00 ± 0.96	7.12 ± 0.88	0.83 ± 0.01
BC-L	0.97 ± 0.12	2.03 ± 0.28	12.3 ± 1.78	0.33 ± 0.03
BC-H	0.98 ± 0.02	2.69 ± 0.44	14.5 ± 3.51	0.47 ± 0.01

699

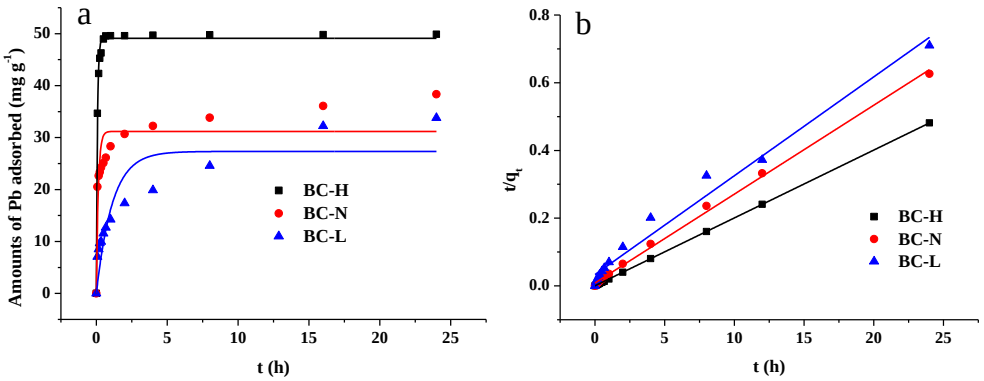

700

701 **Fig. S1.** Kinetics of Pb sorption on SBCs, a) pseudo-first-order kinetic model; b) pseudo-second-order kinetic

702 model.

703

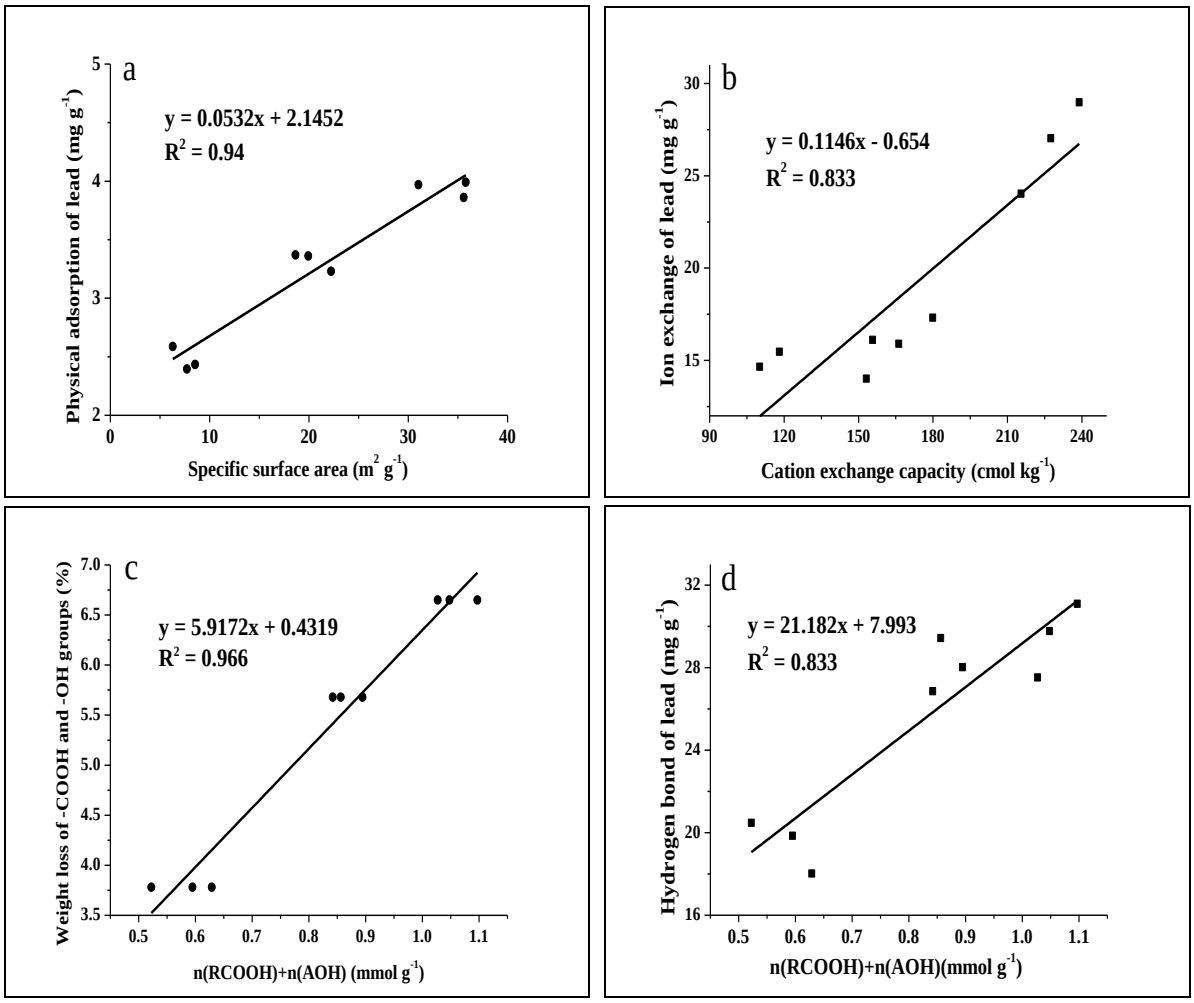

Fig. S2. Correlations between the amount of Pb in different fractions on Pb-loaded SBCs and specific properties of SBCs. a) physical adsorption fraction vs. specific surface area; b) ion exchange fraction vs. CEC; c) weight loss of −COOH and –OH groups on SBCs vs. the sum content of RCOOH and AOH functional groups on SBCs; and d) hydrogen bonding fraction vs. the sum content of RCOOH and AOH functional groups on SBCs.

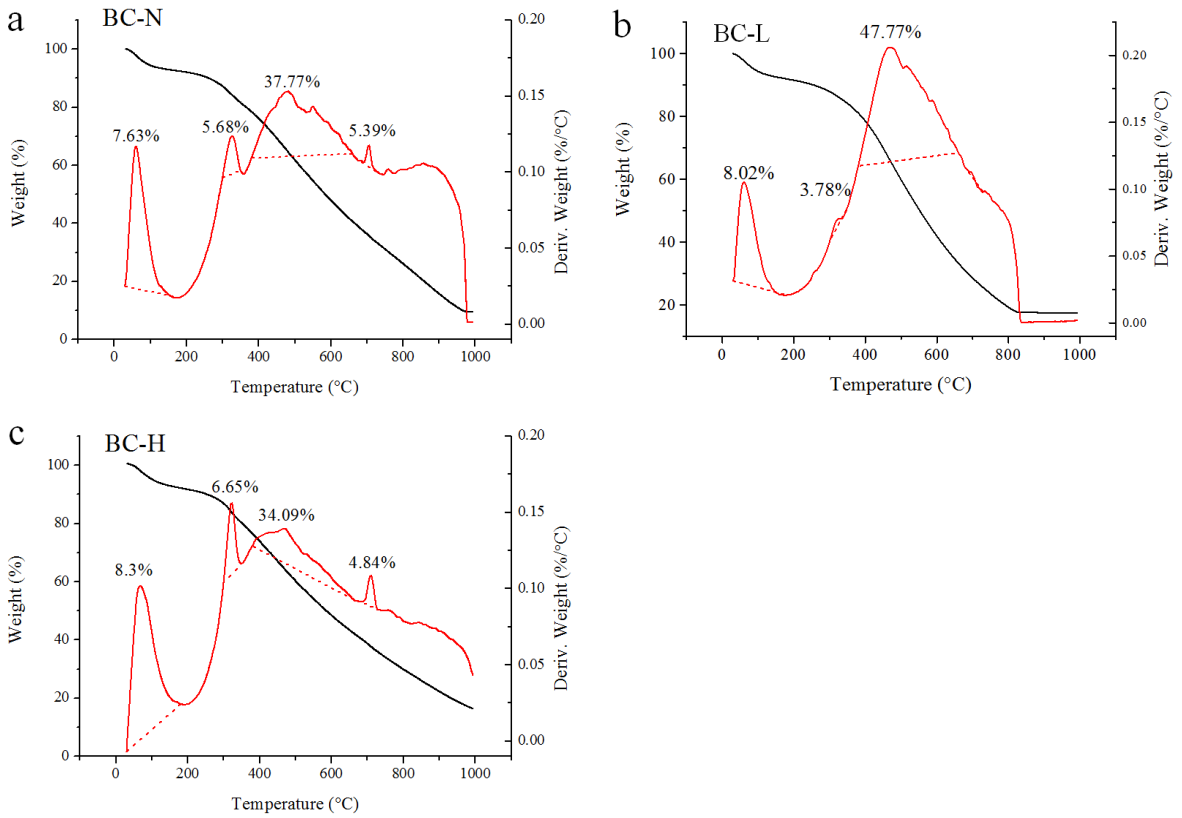

711

712

713 Fig. S3. Thermogravimetric (TG, black line) and differential thermogravimetric (DTG, red line) curves of SBC samples: a)

714 BC-N, b) BC-L, and c) BC-H.

715

716 **References**

717 Inyang, M., Gao, B., Ding, W., Pullammanappallil, P., Zimmerman, A.R., Cao, X.D., 2011. Enhanced lead
718 sorption by biochar derived from anaerobically digested sugarcane bagasse. Sep. Sci. Technol. 46(12),
719 1950–1956. https://doi.org/10.1080/01496395.2011.584604

720 Inyang, M., Gao, B., Yao, Y., Xue, Y.W., Zimmerman, A.R., Pullammanappallil, P., Cao, X.D., 2012. Removal
721 of heavy metals from aqueous solution by biochars derived from anaerobically digested biomass. Bioresour.
722 Technol. 110, 50–56. https://doi.org/10.1016/j.biortech.2012.01.072

723 Li, C., Zhang, L., Gao, Y., Li, A., 2018. Facile synthesis of nano ZnO/ZnS modified biochar by directly
724 pyrolyzing of zinc contaminated corn stover for Pb(II), Cu(II) and Cr(VI) removals. Waste. Manage. 79,
725 525−637. https://doi.org/10.1016/j.wasman.2018.08.035

726 Li, J., Zheng, L., Wang, S.-L., Wu, Z., Wu, W., Niazi, N.K., Shaheen, S.M., Rinklebe, J., Bolan, N., Ok, Y.S.,
727 Wang, H., 2019. Sorption mechanisms of lead on silicon-rich biochar in aqueous solution: Spectroscopic
728 investigation. Sci. Total Environ. 672, 572-582. https://doi.org/10.1016/j.scitotenv.2019.04.003

729 Mohan, D., Pittman, C.U., Bricka, M., Smith, F., Yancey, B., Mohammad, J., Steele, P.H., Alexandre-Franco,
730 M.F., Gomez-Serrano, V., Gong, H., 2007. Sorption of arsenic, cadmium, and lead by chars produced from
731 fast pyrolysis of wood and bark during bio-oil production. J. Colloid. Interf. Sci. 310(1), 57–73.
732 https://doi.org/10.1016/j.jcis.2007.01.020

733 Zhao, T., Yao, Y., Li, D., Wu, F., Zhang, C., Gao, B., 2018. Facile low-temperature one-step synthesis of pomelo
734 peel biochar under air atmosphere and its adsorption behaviors for Ag(I) and Pb(II). Sci. Total Environ.
735 604−601, 73−79. https://doi.org/10.1016/j.scitotenv.2018.05.251

736